



Improved Settling Mechanisms of an Industrial Copper Smelting Slag by CaO Modification

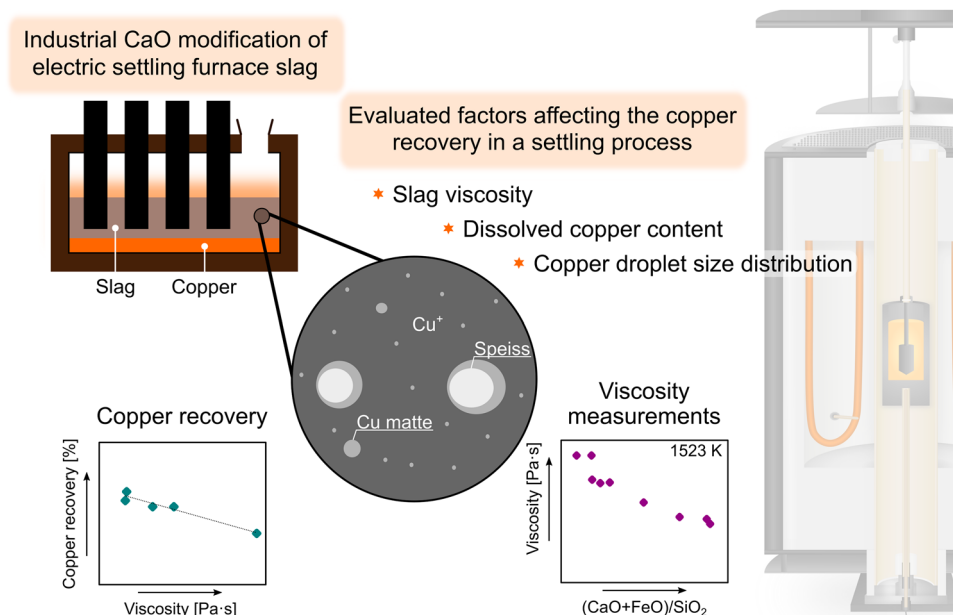
Jenny Isaksson¹ · Anton Andersson¹ · Tommy Vikström² · Andreas Lennartsson¹ · Caisa Samuelsson¹

Received: 30 May 2023 / Accepted: 9 August 2023 / Published online: 28 August 2023
© The Author(s) 2023

Abstract

A significant source of copper losses from pyrometallurgical copper extraction is attributed to dissolved and entrained copper in discarded slag. Entrained copper can be recovered via pyrometallurgical slag cleaning in a settling furnace, where the slag viscosity and copper droplet size distribution (CDS) are critical parameters. Reduced copper losses suggest improved raw material efficiency, and the slag becomes a more environmentally safe byproduct. In this study, iron silicate slags from a smelting furnace are industrially CaO modified in a fuming furnace to contain a CaO content between 8 and 18 wt.%. The viscosity of slags with and without CaO modifications is evaluated in the temperature range from 1423 to 1723 K. The influences of the CaO modifications on the CDS, slag matrix copper content, and total copper content were determined. The results show that the slag viscosity decreases with increasing CaO concentrations in the slag. In addition, the copper content decreases in the slag phase, and the CDS shifts to contain relatively larger droplets. The effect of CaO slag modification reveals a linear relationship between the overall copper recovery and viscosity, which increased from 63 to 88% when the viscosity in the respective batch was 0.51 and 0.25 Pa·s.

Graphical Abstract



Keywords Viscosity · Copper droplets · Size distribution · Iron silicate slag · Dissolved copper · Copper recovery

The contributing editor for this article was Il Sohn.

Extended author information available on the last page of the article

Introduction

During the pyrometallurgical extraction of copper, a significant source of copper loss is discarded slag. In 2021, the global smelter production of copper reached 21.4 million tons [1], and the slag produced was approximately 2.2 tons per ton of copper [2]. The most considerable amounts of slag come from the smelting furnace and often have a copper content between 1 and 2 wt.% [3], resulting in a significant amount of copper in the discarded slag. Copper in the slag is attributed to entrained droplets and dissolved copper. The entrained copper droplets in a slag treated in a fuming furnace are mainly copper matte and speiss, a metalloid mainly containing copper and small amounts of nickel, antimony, arsenic, and iron [4]. Determining factors for the final slag copper content, regarding settling, are slag viscosity, copper droplet size, and the density differences between the copper droplets and the slag [5–7]. Larger droplets settle at a higher rate due to their greater mass and, thus, gravitational force, and a lower viscosity means less internal friction in the liquid and, thus, higher settling rate. Both factors are, thus, crucial properties for recovery in the pyrometallurgical extraction of copper.

The entrained droplets can be recovered in slag-cleaning operations, such as in a settling furnace, where entrained droplets settle through molten slag under gravity. A possible method for decreasing copper losses to slag is to modify the slag to enhance the essential properties and increase the settling rate. Reduced copper losses increase smelter profits by improving the raw material efficiency to enhance the sustainability of copper extraction.

Another driving force to decrease the contents of copper and its associated elements in the slag is the potential hazard of granulated slag, which can mitigate the need for landfills and make utilization as a secondary resource, construction material, or blasting abrasive media. A leaching study of granulated slag has shown that granulated slag exhibits natural leaching of Zn, Cu, and Ni [8]. Other leaching studies have concluded that most of the leached Ni and Sb originate from the speiss phase [9] and that the leaching of As and Sb decreased when granulated iron silicate slag was CaO modified [10]. These elements are associated with the speiss phase in the slag, suggesting that an improved settling and reduced copper content decrease the risk of leaching into the environment and contribute to sustainability and a circular economy. The effects of industrial slag modification, including viscosity data, mineralogy, dissolved copper content, and copper droplet size distribution (CDS), are essential for metal recovery.

The slag viscosity can be measured with a high-temperature rheometer and depends on the temperature, atmosphere, slag composition, and structure. Molten silicate

oxide systems consist of three-dimensional networks of SiO_4^{4-} tetrahedra [11]. The structures of silicate-based melts are affected by (i) the degree of polymerization of the silicate network, (ii) the fitting of certain cations, e.g., Al^{3+} , and (iii) the nature of network-breaking cations, e.g., Ca^{2+} and Mg^{2+} [12]. The gradual addition of basic oxides results in the progressive breaking of the bridging oxygen in the silicate network and the formation of nonbridging and free oxygen. Thus, smaller structural units are present in slag, reducing the viscosity.

Slag from copper smelting furnaces usually contains the oxides FeO and SiO_2 , smaller amounts of Al_2O_3 , CaO, and MgO, and minor elements, such as Cu, As, Sb, Sn, and Pb [13–16]. In the literature, the effects of CaO on the slag properties and the slag copper content have mainly been studied on synthetic materials or slag samples collected in the industry and then modified in a laboratory. The effects of CaO addition on the viscosity have been examined with similar results, where the viscosity decreases with CaO addition [17–23]. The theory behind the reduced viscosity is that the basic oxide CaO breaks the silicate polyions into relatively small structural units, decreasing the viscosity.

The CaO modification of an iron silicate slag system also influences the copper solubility, which decreases with the addition of CaO [24, 25]. A decreased copper solubility enhances the recovery as more dissolved copper becomes entrained and is available for settling. However, one criterion of the entrained droplets to settle within a given time is that they are large enough. The distribution and portion of copper-bearing phases in a fayalite copper slag were studied when the copper content was approximately 0.9 wt.%, the copper-bearing droplets had a particle size distribution ranging from the micrometer scale to the millimeter scale [26]. A study evaluating the effects of experimentally modified slag on the copper size distribution in a slag related to the copper converter shows that larger droplets are obtained when the slag is modified with gypsum and carbon [27]. Droplets that are a few micrometers in diameter take a long time to settle and end in the final slag product if they do not have time to settle completely.

The interfacial tension of matte and slag is suggested to be the primary factor determining the droplet size in a smoothed particle hydrodynamics study, where the droplet size increases with increasing interfacial tension [28]. The surface tension of the slag increases with the addition of CaO [19, 29]. This finding indicates that the CDS can be shifted if the slag is modified. However, a knowledge gap that needs to be studied is what happens with the CDS when the slag is industrially modified with CaO in a slag-cleaning route, including a fuming furnace and a settling furnace. Larger droplet size and lower viscosity suggest a higher settling rate and, thus, an enhanced recovery.

In order to assess the impact of industrial CaO modification of iron silicate slag in a settling furnace, a comprehensive perspective is essential. This involves understanding factors such as slag viscosity, CDS, slag matrix copper content (dissolved copper), and correlations with copper recovery. The standard method for evaluating melt modification is to work with synthetic oxide systems or to collect industrial slag samples and modify them in an experimental environment. This study examines the impact of industrial-scale CaO slag modification on a settling operation. Slag with and without CaO modification (2–18 wt.% CaO) was evaluated, including rheological studies from 1423 to 1723 K in an argon atmosphere. The CDS of one reference batch and one CaO-modified batch (18 wt.% CaO) were investigated using automated mineralogy and SEM–EDS (scanning electron microscope equipped with energy dispersive X-ray spectroscopy), and the slag matrix copper content was estimated using LA-ICP-MS (laser ablation (LA)–inductively coupled plasma–mass spectroscopy (ICP–MS) (LA–ICP–MS)). The CaO modifications were also evaluated by comparing the final copper content and recovery in the settling operation. The findings from the study can be applied industrially to improve slag cleaning and increase raw material efficiency and slag valorization by reducing the copper content and associated elements, improving the sustainability of pyrometallurgical copper extraction.

Experiment

Materials

Industrial slag modification occurred batchwise in a fuming furnace where electric smelting furnace slag was treated under reducing conditions to recover zinc [30]. After finalizing the process, the slag was tapped with a slag runner from the fuming furnace into a settling furnace, where the slag was held as entrained copper droplets settled. The slag was then tapped, water-granulated, and transported to dewatering basins. The copper content was analyzed in slag samples from four sample points: (1) *incoming* slag, a sample taken while tapping the fuming furnace into the settling furnace, (2) *furnace* slag, a sample taken within the settling furnace, (3) *outgoing* slag, a sample taken while tapping the settling furnace, and (4) *granulated* slag, a sample taken from the water-granulated slag.

The incoming and outgoing samples were collected with steel scoops lowered into the slag stream and cooled in ambient air. Reference samples without slag modification were named R1–R5. In addition, samples were collected from four batches modified with limestone (CaCO₃) provided by Nordkalk AB, Sweden. The added CaCO₃ underwent calcination during fuming, and the additions were targeted to reach

10, 15, and 20 wt.% CaO (named C8, C13, C14, and C18, respectively, based on the analyzed CaO content). Details of the slag cleaning and a trial description could be found in previous studies [4, 31].

The incoming and furnace samples were analyzed in a certified laboratory (ALS Scandinavia AB, in Sweden). The samples were analyzed with a Thermo Finnigan Element 1 inductively coupled plasma–sector field mass spectrometry (ICP–SFMS) instrument (Thermo Fisher Scientific, Waltham, MA, USA). The incoming and outgoing slag and the water-granulated slag were analyzed in a smelter laboratory with a standardized method that uses a Philips PW2606 X-ray fluorescence (XRF) instrument (Malvern Panalytical, Malvern, U.K.). The assays were normalized to 100 wt.%. Multiple samples were collected from each batch to obtain reliable results by taking an average of samples.

Viscosity Measurements

The rheological measurements of industrial slag were performed using a rotating cylinder technique and a Mo spindle and crucible (tzm molybdenum 364). The rheometer system was an Anton Paar furnace rheometer system (FRS; FRS 1800) [32]. Before viscosity measurements, the incoming slag samples were crushed, ground, packed into Mo crucibles, and remelted in a Ruhstrat resistance furnace in a N₂ (99.996% purity) and Ar (99.999% purity) atmosphere. Both gases were supplied by Linde Gas AB, Sweden. The flow rates of N₂ and Ar were 12 L/min and 3 L/min, respectively. The heating rate was 5 K/min to 1273 K, and the material was held at this temperature for 30 min; then, the temperature was heated to 1523 K and maintained for an additional 30 min. The material was cooled with the natural cooling of the furnace.

The experimental assembly for rheological measurement is shown in Fig. 1. The crucibles were attached to a hollow Al₂O₃ crucible shaft covered with a graphite sleeve to prevent oxygen from entering the system. The temperature registered during viscosity measurements was measured with a B-type thermocouple positioned in the hollow Al₂O₃ crucible shaft approximately 5 mm from the melt. Ar (99.999% purity, supplied by Linde Gas AB, Sweden) was introduced to the furnace via the crucible shaft using a constant flow rate of 2.5 L/min.

The furnace temperature was first increased to the highest experimental temperature: 1723 K (1450 °C). The spindle was lowered to the measurement position, 9 mm above the crucible bottom. The furnace temperature was kept at the highest temperature for 60 min while rotating the spindle at a shear rate of 2 s⁻¹ to achieve a homogeneous temperature in the melt. A constant viscosity at a fixed shear rate indicated that the melt homogenized. The viscosity was measured during the cooling cycle in 50 K increments from 1723 to

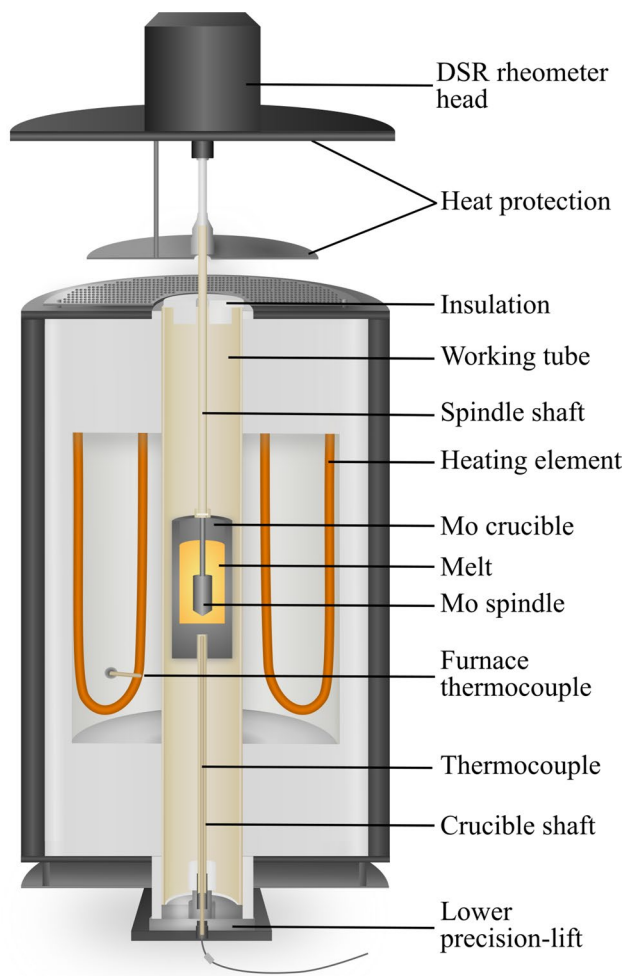


Fig. 1 Anton Paar FRS 1800 high-temperature rheometer

1423 K. At a new temperature (1723–1523 K), the furnace temperature was held for 45 min using a shear rate of 4 s^{-1} for homogenization and at least 60 min at the final two temperatures, as it took longer to obtain stable measurements. Afterward, an automated program measured the viscosity with shear rates of 1, 2, 4, 8, and 16 s^{-1} . After finalizing the measurements, the sample cooled alongside natural furnace cooling while maintaining the Ar atmosphere. In this setup, it was not possible to quench the samples.

The rheometer was calibrated under controlled conditions using reference oils by Anton Paar. The performance of the furnace rheometer system was controlled by measuring the viscosity in Standard Glass 1 of the Deutsche Glastechnische Gesellschaft (DGG1) with a viscosity of $93.2 \text{ Pa}\cdot\text{s}$ at 1473 K.

Copper Droplet Size Distribution

Pieces of the incoming slag from batches R3 and C18 were mounted in epoxy, polished using a standard metallographic procedure and carbon coated. The main difference between

Table 1 Overview of the analyses and samples collected during the industrial trial

Slag Sample	ICP–SFMS	XRF	Viscosity	LA–ICP–MS	CDS
Incoming	X	X	X		X
Furnace	X	X			
Outgoing		X			
Granulated		X		X	

these samples was the CaO content. The CDSs of the copper phases were analyzed using automated mineralogy and quantitative target mineralogy (QanTmin) SEM, Zeiss Sigma 300 VP (Zeiss, Oberkochen, Germany). The compositions of the droplets were analyzed using two Bruker Instrument EDS detectors (Bruker, Billerica, United States) and Zeiss Mineralogic software (Zeiss, Oberkochen, Germany). The step size during the measurements was $0.7 \mu\text{m}$, and the working distance was 8.5 mm. The SEM had an accelerating voltage of 20 keV and an emission current of 1 nA.

Copper Content in the Slag Matrix

The Cu content in the slag matrix (oxide phase), which was visually free from copper droplets, was determined using LA–ICP–MS. The samples used in the analysis were water-granulated from batches R4, C8, C13, and C18. For this purpose, an ESL NWR193 LA system and a ThermoScientific iCAPQ ICP–MS were utilized. NIST 610 was used as the reference material, and the quality assurance/quality control protocol was conducted with NIST 612. The silicon content in the oxide phase was analyzed using a Zeiss Gemini Merlin SEM (Zeiss, Oberkochen, Germany) and an Oxford Instrument X-Max EDS (Oxford Instruments, Abingdon, U.K.) detector. The SEM had an accelerating voltage of 20 keV, an emission current of 1 nA, and a working distance of 8.5 mm. Before analysis, beam measurement calibration for EDS was performed on pure copper. The elemental compositions were reported in wt.% and normalized, suggesting that the sum of the elements was 100 wt.%. The silicon content from the EDS analysis was used as the internal standard in the subsequent data reduction procedure performed with Iolite 4.

Results and Discussion

Slag samples were collected from four sampling points during the industrial settling furnace trial, (1) *incoming*, (2) *furnace*, (3) *outgoing*, and (4) *granulated* slag. An explanation of the sample procedure and position was given in the Materials section. Table 1 gives an overview of the samples and performed analyses.

Chemical Composition

Table 2 presents the average chemical compositions, FeO/SiO₂, and (CaO + FeO)/SiO₂ ratios (wt.%/wt.%) of the incoming samples. The CaO content varied from 2.3 to 3.9 in the reference batches (R1–R5) and 7.7–18.3 wt.% in the CaO-modified batches. The FeO/SiO₂ ratio was 1.3 for all batches except for C18, and the (CaO + FeO)/SiO₂ ratios varied between 1.34–1.70. The total copper content varied between 1.0 and 1.6 wt.%, including the chemically dissolved and entrained copper. The operational conditions and the separation between the slag and matte phases in the smelting furnace, i.e., the unit operation before the fuming furnace, determined the copper content in each batch. The total copper, iron, chromium, and molybdenum contents are presented as FeO, Cr₂O₃, and Mo, respectively. However, the valence state was not confirmed.

Viscosity Measurements

The viscosity measurements between 1723 and 1473 K (± 3 K) are shown in Fig. 2. The shear rate used when collecting the viscosity data was 8 s⁻¹, and the presented viscosity was an average of 60 measurement points. The sample standard deviation was at most 1%. In all cases, the viscosity decreased with increasing temperature. R1 and R2 showed no significant differences in the viscosity data over the entire temperature range. R5 differed from R1 and R2 at the two lowest temperatures (1473 and 1523 K), and R3 and R4 differed from all batches. R4 had the lowest FeO/SiO₂ ratio among the reference batches. However, trends between the viscosity and composition for the reference batches are difficult to distinguish as the slag composition was not controlled during the trial and had a natural variation due to the feed of copper concentrates, slag returns, slag formers, secondary raw materials, and other additions. The viscosity measurements of R1–R5, thus, showed viscosity variations during normal operation.

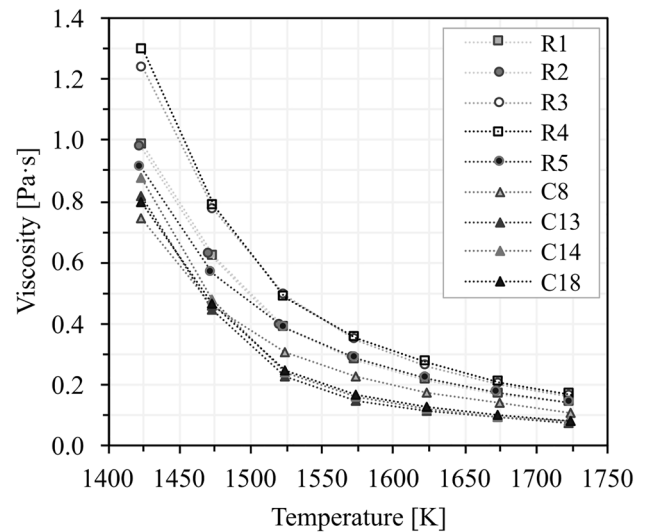


Fig. 2 Viscosity plotted against the temperature (1473–1573 K ± 3 K)

Batches modified with CaO had lower viscosities than the reference batches (R1–R5). The temperature range between 1523 and 1573 K was evaluated carefully, as this range is often used in industrial slag-cleaning operations, such as those in a settling furnace. The (CaO + FeO)/SiO₂ ratio vs. viscosity (1523 and 1573 K) is shown in Fig. 3. The viscosity was lower in batches with higher (CaO + FeO)/SiO₂ ratios, and the effect was most pronounced between 1.43 and 1.61. At relatively high ratios (above 1.61), no significant effects were observed in the viscosity data. At the lowest temperature of 1523 K, C13 had the lowest viscosity of 0.45 Pa·s, and R4 had the highest viscosity of 0.78 Pa·s, 1.75 times higher than that of C13. The viscosity of R5, which had the lowest viscosity among the reference batches, at the same temperature was 1.26 times higher than that of C13.

In earlier studies, the effect of the Fe/SiO₂ ratio on the viscosity was studied, showing that viscosity decreased with increasing ratio [33–35]. The viscosity decreased because

Table 2 Normalized chemical composition, FeO/SiO₂, and (CaO + FeO)/SiO₂ ratios of batches collected during normal operation (R1–R5) and CaO-modified batches (C8–C18)

Sample	[wt.%/wt.%]		[wt.%]								
	FeO/SiO ₂	(CaO + FeO)/SiO ₂	SiO ₂	FeO	Al ₂ O ₃	CaO	MgO	ZnO	Cu	Cr ₂ O ₃	Mo
R1	1.32	1.43	37.8	50.0	4.4	3.9	1.1	1.3	1.2	0.2	0.2
R2	1.30	1.38	38.2	49.6	4.9	3.0	1.3	1.4	1.3	0.2	0.2
R3	1.30	1.38	38.9	50.4	4.1	3.1	1.1	1.1	1.0	0.1	0.2
R4	1.26	1.34	39.3	49.4	4.7	3.1	1.2	0.7	1.1	0.2	0.2
R5	1.34	1.40	38.7	51.8	3.6	2.3	1.1	0.7	1.4	0.1	0.2
C8	1.30	1.52	36.4	47.5	4.8	7.7	1.2	0.7	1.3	0.2	0.2
C13	1.27	1.69	33.9	44.2	4.5	13.2	1.5	1.0	1.3	0.2	0.2
C14	1.31	1.70	34.0	43.2	4.4	14.1	1.8	0.6	1.5	0.3	0.2
C18	1.09	1.61	35.0	38.2	4.2	18.3	1.5	0.9	1.6	0.2	0.2

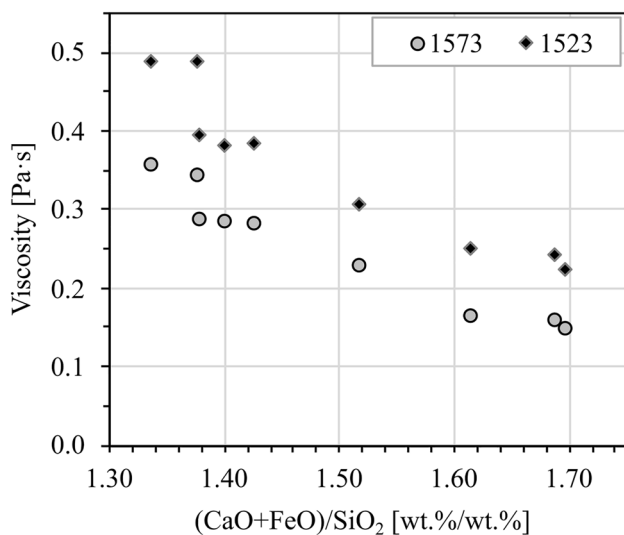


Fig. 3 Viscosities at 1523 and 1573 K vs. (CaO+FeO)/SiO₂ ratio (wt.%/wt.%). The temperature was within an accuracy of ± 3 K

FeO is a network modifier that could decompose to produce free oxygen that breaks the silicate network into smaller structural units [36, 37]. The effect of CaO content on the viscosity has been examined with similar results, decreasing when CaO addition increased [17–23]. The melt has less potential of breaking the silicate network if the (CaO+FeO)/SiO₂ ratio is low, meaning that the viscosity is relatively high due to the polymerization of the silicate network.

Viscosity measurements were performed at each temperature using different shear rates ranging from 1 to 16 s⁻¹. At 1724 K, the viscosity curves decreased with increasing shear rates, a non-Newtonian shear-thinning behavior. The shear-thinning behavior was most pronounced for samples C14 and C18. At the lowest temperature, all melts showed Newtonian behavior, suggesting that the shear rate did not influence the viscosity data. The main differences between the measurements were the temperature and time (9 h) between the measurements. The samples were collected from a slag-cleaning route before a settling furnace, indicating that the slag was not homogeneous and contained entrained copper droplets and solid phases that settle with time [4]. When the shear rate increased, particles in the melt were favorably oriented, suggesting that the viscosity decreased.

Relatively large droplets (millimeter scale) were found at the bottom of the crucible when cutting them after the measurement. The large droplets indicated that the relatively small copper-containing droplets settled and coalesced during viscosity measurement. The settling during the rheological measurements was confirmed in the post-experimental analysis, where the copper content was between 0.3 and 0.2 wt.%. After rheological measurements, a post-experimental analysis of the samples showed that the Mo content was

between 0.5 and 1.3 wt.%, higher in the CaO-modified samples.

Activation Energy

The viscosity of liquids decreases with increasing temperature [33, 38, 39]. The temperature dependence of the viscosity for a given melt composition can be described by an Arrhenius-type relationship [40], as shown in Eq. 1.

$$\eta = A \exp\left(\frac{E_a}{RT}\right), \quad (1)$$

where η is the viscosity in Pa·s, A is the preexponential factor (Pa·s), E_a is the activation energy of flow in J/mol, T is the absolute temperature in K, and R is the gas constant (8.341 J/mol·K). The activation energy for viscous flow is the energy required to break the bonds necessary for viscous flow and consequently reflects the effects of structure on physical properties [12, 41]. The logarithm of the Arrhenius equation provides a linear relationship between $\ln(\eta)$ and $1/T$. A linear relationship of the measured data indicates that the material is fully liquid and that the melt follows an Arrhenius behavior. Deviations from a linear system may occur due to solid phases in the melt. Roscoe developed a model based on Einstein's approach, titled the Einstein–Roscoe equation, which describes the viscosities of melts with solid particles [42–44], showing that the melt viscosity increases with solid particles present.

When the Arrhenius equation is applied to the viscosity data, it is seen that C13, C14, and C18 deviate from the behaviors of R1–R5 and C8. The different behaviors of the two groups are exemplified in Fig. 4a and b, represented by samples R2 and C13, respectively. The figures show the natural logarithm of the viscosity vs. the temperature inverse, trendline, and R^2 values. When all measurements (entire temperature interval) are included, the trendline (dotted) for C13 has a lower R^2 value than that for R2 (0.96 and 0.99, respectively). This difference arises because the slope was relatively steep for the C13 data and less steep for the R2 data at temperatures of 1524 K and lower. The data are, thus, divided and plotted separately at the temperature intervals 1724–1574 and 1524–1474 K to reveal the significant difference in the slope. The deviations from the Arrhenius behaviors for C13, C14, and C18 indicate that structural changes appear below 1524 K. The pronounced temperature dependence of the viscosity was indicated by the homogenization times at these temperatures, which took up to 75 min. The increased time for the melt to become homogeneous implies structural changes or solid precipitation at low temperatures.

The activation energies for the two temperature intervals, 1574–1724 K and 1424–1524 K, are plotted against the (CaO + FeO)/SiO₂ ratio in Fig. 5a and b, respectively.

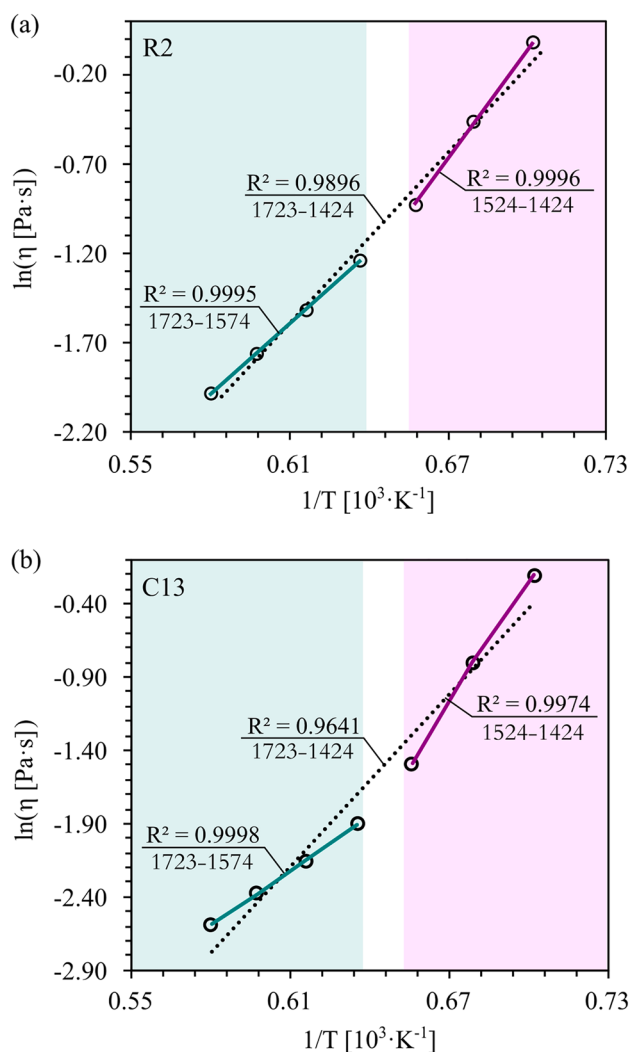


Fig. 4 $\ln(\text{viscosity [Pa}\cdot\text{s]})$ vs. the inverse of the temperature ($1/T$) for **a** R2 and **b** C13. The calculations were performed for three temperature intervals to highlight deviations from the Arrhenius equation and linearity. The dotted trendline is for the entire temperature interval. In each figure, the green trendline to the left is between 1574 and 1723 K, and the purple trendline to the right is between 1424 and 1524 K (Color figure online)

The activation energy for the reference batches (R1–R5) varies between 156 and 170 kJ/mole in the low-temperature (1424–1524 K) interval and between 107 and 115 kJ/mole in the high-temperature interval (1574–1724 K). The variation in the activation energy of the reference batches reflects the compositional variations during normal operation in the fuming furnace without CaO modifications. At the high-temperature interval, the activation energy of the CaO-modified batches varied between 103 and 111 kJ/mole, approximately the same as that for the reference batches. However, a correlation can be observed, where the activation decreases with increasing ratio. The trend shifts in the low-temperature interval, showing that the activation energy

is significantly higher in batches with a CaO content above 13 wt.% (C13–C18) than in the reference batches and C8. The activation energy is between 209 and 233 kJ/mole for C13–C18 and 159 kJ/mole for C8.

The difference in activation energy for the two intervals implies structural changes, solid precipitation, and increased viscosity-temperature dependence of the melt in the low-temperature interval. All batches can be assumed to be fully liquid in the high-temperature interval. When translating this assumption to an industrial perspective, batches with CaO contents higher than 13 wt.% should preferably be operated above 1524 K to avoid solid precipitation and, thus, a more viscous slag. Solid particles in the slag can hinder settling, as they can attach to copper droplets, forming a copper-solid entity with a lower average density than the copper phase [4, 45–47]. The lower density of the copper-solid entity results in accumulation above the settled copper phase in a settling furnace.

Copper Content in the Slag Matrix

The total copper content in the industrial slag is the sum of entrained and dissolved copper in the slag matrix. The total copper contents are analyzed in slag samples after the settling (*furnace, outgoing, and granulated slag*). The total slag copper content is an average of these samples for each batch. The copper content in the oxide phase is estimated using LA-ICP-MS. The samples were granulated and, thus, cooled quicker than those collected while tapping, limiting the precipitation of dissolved copper. The precipitation of dissolved copper can cause the entrainment of copper droplets due to decreased solubility in the slag [48]. The precipitation of copper can be induced during slag cooling by the reaction between copper oxide and iron oxide, forming metallic copper and ferric iron [49, 50]. The precipitated metallic copper disperses throughout the slag layer as fine droplets.

The total and entrained copper content and the dissolved copper content in the oxide phase are plotted against the CaO content in Fig. 6a. The plot reveals that the total copper content is lower in the batches modified with CaO. The entrained copper content is estimated as the difference between the total and dissolved copper contents. The dissolved copper content varies between 0.35 and 0.48 wt.%, lowest in C13 and highest in the batch without CaO modification (R4), indicating that the dissolved copper content in the slag decreases when the slag is modified. The decreased copper solubility can be explained by the acid–base theory of slags, where Ca^{2+} ions replace Cu^{+} ions within the slag structure [24]. A decreased copper solubility enhances recovery as dissolved copper becomes entrained and is available for settling.

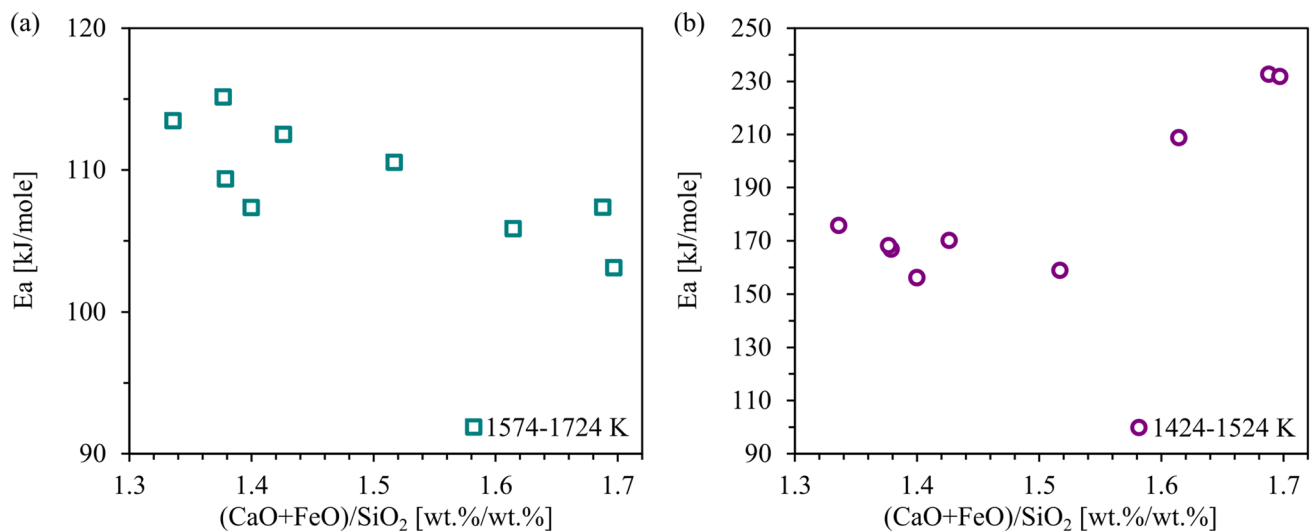


Fig. 5 Activation energy plotted against the $(\text{CaO} + \text{FeO})/\text{SiO}_2$ ratio in the temperature intervals **a** 1574–1724 K and **b** 1424–1524 K. The melts in the high-temperature interval can be assumed to be fully liquid

The copper recovery is calculated by subtracting the outgoing copper content from the incoming copper content and dividing it by the incoming copper content—the mass difference between the slag before and after settling is assumed to be negligible. The temperature for the batches varies between 1496 and 1525 K, lowest for C13 and highest for C8. The copper recovery of the entrained copper content (droplet recovery) is calculated by subtracting the dissolved copper content from the incoming and outgoing copper contents and then using the same calculation for the total copper recovery. The total and droplet copper recovery data are plotted against the viscosity at the actual settling process temperature in Fig. 6b. The plot reveals a clear trend where the copper recovery is higher in the batches with a lower apparent viscosity during processing.

Copper Droplet Size Distribution

The CDS (Copper Droplet Size Distribution) was evaluated in slowly cooled incoming slag samples to the settling furnace. The CDS analysis revealed that copper droplets settled in the molten slag after sampling and before solidifying. The settling was indicated by a gradient of CDSs in the samples, as exemplified in Fig. 7. For R3, large droplets reaching 216 μm in size were frequently found near the bottom of the slag piece, indicating that settling occurred and emphasizing the importance of droplet size regarding settling rates. The illustration only focuses on the copper droplets and does not reflect the appearance of the liquid slag phase and possible solids.

The cumulative CDSs (%) of R3 and C18 are shown in Fig. 8, with the cumulative area % of each size fraction. The CDS for R3 showed that 38% of the droplets were in a

size range below 5 μm , and most of the droplets (90%) were below 15 μm in size. Due to their small sizes, these droplets had low settling rates, suggesting they would be lost with the slag after finalizing the settling. The largest droplets in R3 (100–216 μm) were 0.1% of the total droplets analyzed. The CDS for C18 showed a shifted CDS relative to R3, where 22% of the droplets had diameters of less than 5 μm ; the largest droplets (100–408 μm) were 1.2% of the total droplet count.

The fraction of dissolved copper was calculated in the incoming slag by assuming that the slag matrix copper content in the granulated slag was unchanged during settling and then dividing the dissolved copper content by the incoming copper content. The percentage of dissolved copper in the incoming slag is shown in Fig. 9, revealing that the dissolved copper content was lower in batches modified with CaO: 43% in R4 and 25% in C18. The relatively high content of dissolved copper in a reference batch (43%) explained the high number of droplets with diameters of less than 5 μm detected in R3. The samples were cooled in ambient air, causing the precipitation of dissolved copper due to decreased solubility in slag, suggesting that a fraction of the detected droplets could have been dissolved during the actual process.

The software measured the droplet area, and the cumulative area % for R3 showed that droplets with diameters less than 15 μm accounted for 39% of the total copper droplet area. The droplets with sizes between 100 and 216 μm were 0.1% of the total droplet number. However, the total area of these droplets was 13%, and the area of droplets larger than 50 μm was 22%, suggesting that the droplets (> 50 μm) still contributed to decreased copper content in the final slag as

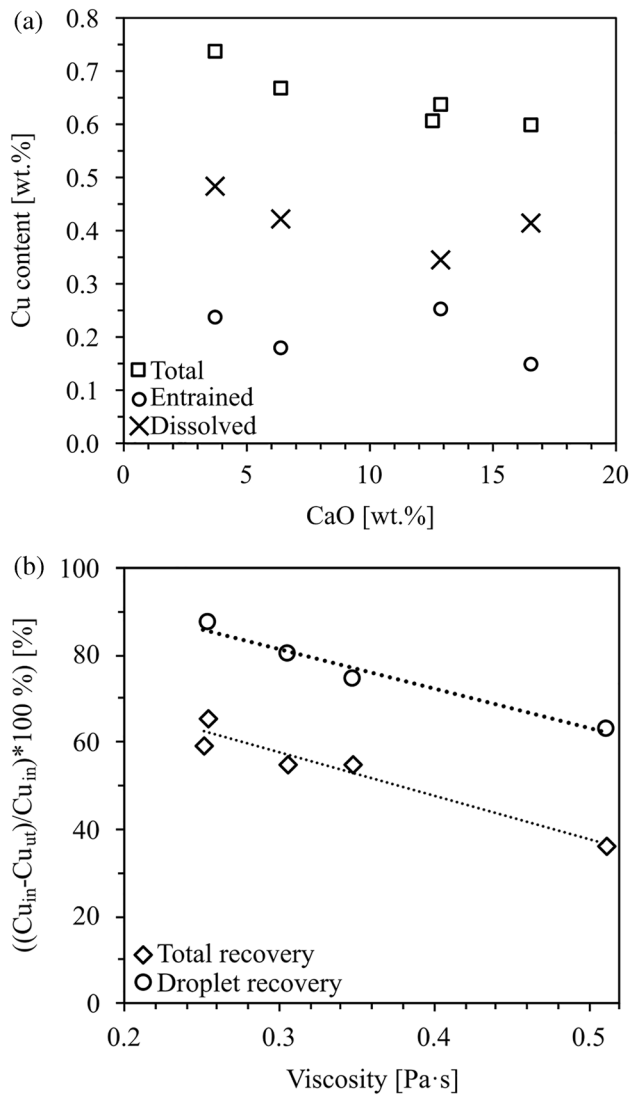


Fig. 6 **a** Total, entrained, and dissolved copper contents in the final slag vs. the CaO content. **b** Total recovery and droplet recovery vs. viscosity at the temperature during industrial settling for each batch

they settled with a higher rate. For C18, the cumulative area % differed significantly from R3, where the cumulative area % of the droplets with sizes less than 15 μm accounted for 12% of the total area, and the largest droplets (100–408 μm) accounted for 72%. The results showed that the CaO modification increased the droplet size.

The CaO modification decreased the slag copper solubility [24, 25], indicating that more copper droplets were available for settling. However, the droplets must be sufficiently large to settle to the underlying copper phase before settling ends. The interfacial tension of matte and slag was suggested to be the primary factor determining the droplet size, which increased with increasing interfacial tension [28]. The surface tension of slag was influenced by the addition of CaO, which increased with increasing addition [19, 29]. A

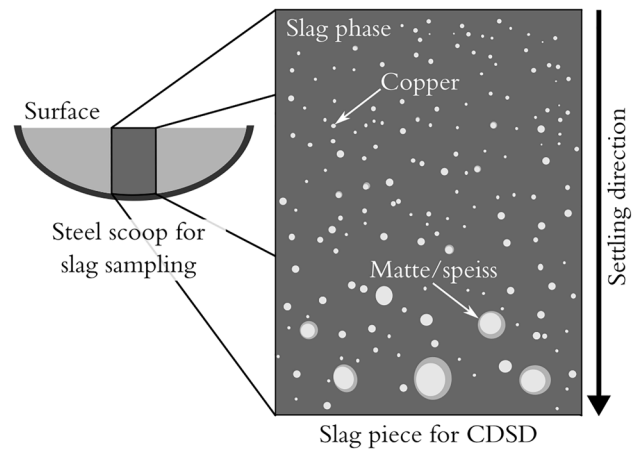


Fig. 7 Schematic figure of the gradient of copper droplets that increased in size toward the bottom of the slag piece

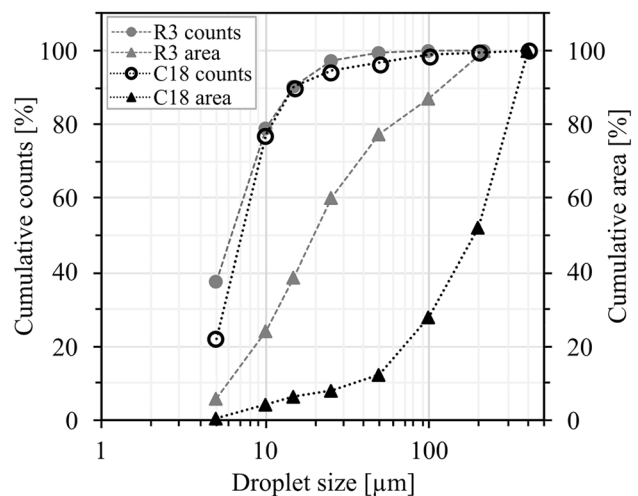


Fig. 8 Cumulative CDS (%) and cumulative area (%) characteristics of copper droplets in R3 and C18

decreased viscosity increases the mobility of the droplets, thus, improving the chance of them coalescing and increasing the droplet size, settling rate, and copper recovery. The CaO modification occurred in the fuming furnace, where the slag was treated under a turbulent flow, suggesting that the entrained droplets had time to coalesce. The tendency for the coalescence of copper droplets should increase with the CaO modification, which was indicated by the CDS evaluation. The droplets were mainly in the form of speiss, matte, and copper sulfide.

The theoretical settling velocity could be estimated with Stokes' law, displayed in Eq. 2, where v is the settling velocity (m s^{-1}), ρ_{Cu} is the density of copper droplets (estimated to be 9000 kg m^{-3}), ρ_{slag} is the slag viscosity (estimated to be 3600 kg m^{-3}), g is the gravimetric acceleration, R is the

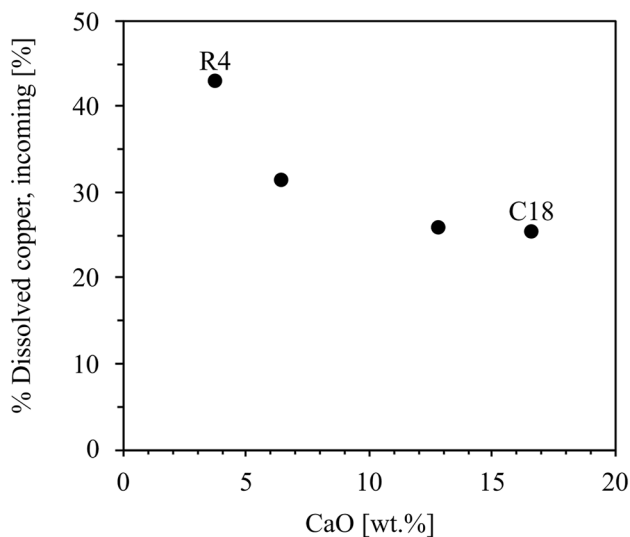


Fig. 9 Percentage of dissolved copper in the incoming slag to the settling furnace

radius of the copper droplets (m), and η is the slag viscosity (Pa·s).

$$v = \frac{2}{9} \left(\frac{\rho_{Cu} - \rho_{slag}}{\eta} \right) gR^2. \quad (2)$$

The settling time was plotted against the cumulative area % of the copper droplets, as shown in Fig. 10, to estimate the influence of the CDS on the settling time. The slag bath heights were 0.5, 0.3, and 0.1 m; the apparent viscosity for the slag was the measured viscosity at the operating temperature registered during the trial. The CDS was assumed

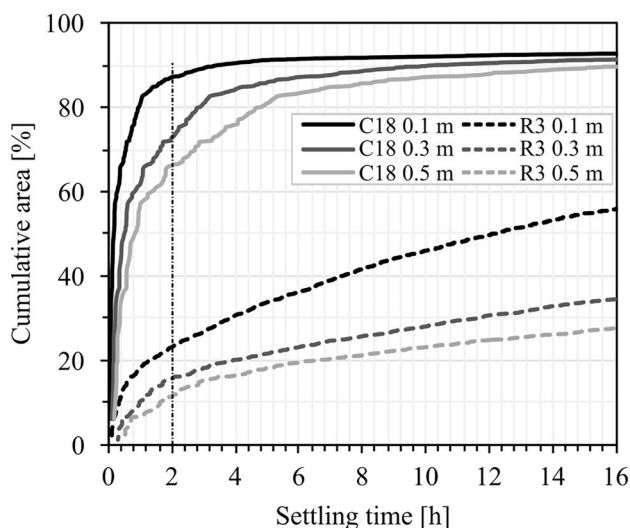


Fig. 10 Settling time for the cumulative area % of the copper droplets in R3 and C18

for the entire slag bath, and the droplets were assumed to be spherical. However, the settling during the operation in the settling furnace was complex, including the settling time with a given slag bath height and stagnant conditions and the slag-tapping process when the slag bath height was dynamic. After the given settling time, the slag was tapped from the furnace while the settling continued. The bath height decreased while tapping, suggesting that the droplets approached the underlying accumulated copper phase. Droplets remaining after the finalization of the settling contribute to the final slag copper content.

The plot revealed that there was a significant difference between R3 and C18. After two hours (vertical line in Fig. 10) of settling, 16% of the droplet area settled from 0.3 m in R3, and 73% settled in C18 from the same distance. The difference between the samples was a combined effect of lower viscosity and a higher CDS in C18. The droplets that settled from 0.5 m within two hours had to be larger than 107 μm in the R3 slag and larger than 94 μm in C18, corresponding to 11% and 66%, respectively. The estimated settling times indicated that many aspects of settling were essential, including the slag bath height, CDS, and slag viscosity. The results showed that CaO was a slag modifier that could be used to enhance settling, which was indicated by viscosity measurements, CDS, and copper recovery in the settling furnace during the industrial settling trial.

Conclusions

In the present study, industrial CaO modification of an iron silicate copper smelting slag was evaluated by performing viscosity measurements, comparing the slag matrix copper content, CDS, final slag copper content after settling, and copper recovery. The main conclusions of the industrial CaO modification were as follows:

- The viscosity was lower in the slag modified with CaO than in the reference slag collected during normal operation.
- The viscosity of the slag with a CaO content above 13 wt.% had a relatively strong dependence on temperature and a relatively high activation energy at temperatures below 1524 K, which was attributed to structural changes and solid precipitation. These batches should preferably be operated at a temperature above 1524 K.
- The copper content in the solidified slag matrix was lower in the batches modified with CaO than in the unmodified batches, indicating that the copper solubility in the slag was lower when the CaO content was between 8 and 18 wt.%.
- Most of the copper droplets (90%) in a reference batch had a diameter smaller than 15 μm , suggesting that these

droplets did not have time to settle during the settling process investigated. The cumulative area of these droplets was 39%.

- The CDSD shifted to contain a higher number of larger droplets when the slag was modified with CaO, enhancing the settling of entrained droplets and copper recovery.
- The copper recovery was strongly correlated to the slag viscosity under the given process conditions, being higher in the slag with lower viscosity.

The conclusions from the study confirmed that industrial slag treated in an electric settling furnace could be modified with CaO for enhanced settling and copper recovery characteristics. The findings could be applied industrially to improve slag cleaning and increase raw material efficiency and slag valorization by reducing the contents of copper and associated elements, improving the sustainability of pyrometallurgical copper extraction.

Acknowledgements The project was conducted within the Center for Advanced Mining and Metallurgy (CAMM) at Luleå University of Technology and financially supported by Boliden AB through Bolidenpaketet.

Funding Open access funding provided by Lulea University of Technology.

Declarations

Conflict of interest The authors declare that they have no conflicts of interest.

Open Access This article is licensed under a Creative Commons Attribution 4.0 International License, which permits use, sharing, adaptation, distribution and reproduction in any medium or format, as long as you give appropriate credit to the original author(s) and the source, provide a link to the Creative Commons licence, and indicate if changes were made. The images or other third party material in this article are included in the article's Creative Commons licence, unless indicated otherwise in a credit line to the material. If material is not included in the article's Creative Commons licence and your intended use is not permitted by statutory regulation or exceeds the permitted use, you will need to obtain permission directly from the copyright holder. To view a copy of this licence, visit <http://creativecommons.org/licenses/by/4.0/>.

References

1. International Copper Study Group (2022) The world copper factbook. <https://icsg.org/copper-factbook/>. Accessed 15 Apr 2023
2. Gorai B, Jana RK, Premchand (2003) Characteristics and utilisation of copper slag—a review. *Resour Conserv Recycl* 39:299–313. [https://doi.org/10.1016/S0921-3449\(02\)00171-4](https://doi.org/10.1016/S0921-3449(02)00171-4)
3. Schlesinger M, King M, Sole K, Davenport W (2011) Extractive metallurgy of copper. Elsevier Ltd, Oxford
4. Isaksson J, Vikström T, Lennartsson A, Samuelsson C (2021) Influence of process parameters on copper content in reduced iron silicate slag in a settling furnace. *Metals* 11:992. <https://doi.org/10.3390/met11060992>
5. Eriç R (2004) Slag properties and design issues pertinent to matte smelting electric furnaces. *J S Afr Inst Min Metall* 104:499–510
6. Stokes GG (1851) On the effect of the internal friction of fluids on the motion of pendulums. *Trans Camb Philos Soc* 9:8. <https://doi.org/10.1017/cbo9780511702242.005>
7. Schmidt A, Montenegro V, Wehinger GD (2021) Transient CFD modeling of matte settling behavior and coalescence in an industrial copper flash smelting furnace settler. *Metall Mater Trans B* 52:405–413. <https://doi.org/10.1007/s11663-020-02026-0>
8. Lidelöv S, Mácsik J, Carabante I, Kumpiene J (2017) Leaching behaviour of copper slag, construction and demolition waste and crushed rock used in a full-scale road construction. *J Environ Manag* 204:695–703. <https://doi.org/10.1016/j.jenvman.2017.09.032>
9. Andertun JK, Samuelsson C, Peltola P, Engström F (2022) Characterisation and leaching behaviour of granulated iron silicate slag constituents. *Can Metall Q* 61:14–23. <https://doi.org/10.1080/00084433.2021.2016345>
10. Andertun JK, Vikström T, Peltola P, Samuelsson C, Engström F (2021) Characterisation and leaching behavior of CaO-modified iron-silicate slag produced in laboratory and industrial scales. *Can Metall Q* 60:294–305. <https://doi.org/10.1080/00084433.2021.201634611>
11. Mysen B, Richet P (2019) Silicate glasses and melts. Elsevier, Amsterdam
12. Mills KC (1993) The influence of structure on the physico-chemical properties of slags. *ISIJ Int* 33:148–155. <https://doi.org/10.2355/isijinternational.33.148>
13. Mackey PJ (1982) The physical chemistry of copper smelting slags—a review. *Can Metall Q* 21:221–260. <https://doi.org/10.1179/cm.1982.21.3.221>
14. Mostaghel S, Samuelsson C, Björkman B (2013) Influence of alumina on mineralogy and environmental properties of zinc-copper smelting slags. *Int J Miner Metall Mater* 20:234–245. <https://doi.org/10.1007/s12613-013-0718-3>
15. Utigard TA (1994) Density of copper/nickel sulphide smelting and converting slags. *Scand J Metall* 23:37–41
16. Shen H, Forssberg E (2003) An overview of recovery of metals from slags. *Waste Manag* 23:933–949. [https://doi.org/10.1016/S0956-053X\(02\)00164-2](https://doi.org/10.1016/S0956-053X(02)00164-2)
17. Kaiura GH, Toguri JM, Marchant G (1977) Viscosity of fayalite-based slags. *Can Metall Q* 16:156–160. <https://doi.org/10.1179/cm.1977.16.1.156>
18. Ducret AC, Rankin WJ (2002) Liquidus temperatures and viscosities of FeO-Fe₂O₃-SiO₂-CaO-MgO slags at compositions relevant to nickel matte smelting. *Scand J Metall* 31:59–67. <https://doi.org/10.1034/j.1600-0692.2002.310108.x>
19. Zhang H, Fu L, Qi J, Xuan W (2019) Physicochemical properties of the molten iron-rich slags related to the copper recovery. *Metall Mater Trans B* 50:1852–1861. <https://doi.org/10.1007/s11663-019-01611-2>
20. Yan Z, Reddy RG, Lv X, Pang Z, Bai C (2019) Viscosity of iron oxide aluminosilicate melts. *Metall Mater Trans B* 50:251–261. <https://doi.org/10.1007/s11663-018-1460-z>
21. Selivanov E, Gulyaeva R, Istomin S, Belyaev V, Tyushnyakov S, Bykov A (2015) Viscosity and thermal properties of slag in the process of autogenous smelting of copper–zinc concentrates. *Miner Process Extr Metall* 124:88–95. <https://doi.org/10.1179/1743285514Y.0000000078>
22. Shen Y, Chong J, Huang Z, Tian J, Zhang W, Tang X, Ding W, Du X (2019) Viscosity and structure of a CaO-SiO₂-FeO-MgO system during a modified process from nickel slag by CaO. *Materials* 12:2562. <https://doi.org/10.3390/ma12162562>
23. Chen M, Zhao B (2015) Viscosity Measurements of SiO₂-"FeO"-CaO System in Equilibrium with Metallic Fe. *Metall Mater Trans B* 46:577–584. <https://doi.org/10.1007/s11663-014-0241-6>

24. Kim HG, Sohn HY (1998) Effects of CaO, Al₂O₃, and MgO additions on the copper solubility, ferric/ferrous ratio, and minor-element behavior of iron-silicate slags. *Metall Mater Trans B* 29:583–590. <https://doi.org/10.1007/s11663-998-0093-z>
25. Holzheid A, Lidders K (2001) Solubility of copper in silicate melts as function of oxygen and sulfur fugacities, temperature, and silicate composition. *Geochim Cosmochim Acta* 65:1933–1951. [https://doi.org/10.1016/S0016-7037\(01\)00545-2](https://doi.org/10.1016/S0016-7037(01)00545-2)
26. Wang X, Geysen D, Padilla Tinoco SV, D'Hoker N, Van Gerven T, Blanpain B (2015) Characterisation of copper slag in view of metal recovery. *Miner Process Extr Metall* 124:83–87. <https://doi.org/10.1179/1743285515Y.0000000004>
27. Gao X, Chen Z, Shi J, Taskinen P, Jokilaakso A (2020) Effect of cooling rate and slag modification on the copper matte in smelting slag. *Min Metall Explor* 37:1593–1601. <https://doi.org/10.1007/s42461-020-00274-x>
28. Natsui S, Nashimoto R, Kumagai T, Kikuchi T, Suzuki RO (2017) An SPH study of molten matte–slag dispersion. *Metall Mater Trans B* 48:1792–1806. <https://doi.org/10.1007/s11663-017-0930-z>
29. Elliott JF, Mounier M (1982) Surface and interfacial tensions in copper matte-slag systems, 1200°C. *Can Metall Q* 21:415–428. <https://doi.org/10.1179/cm.1982.21.4.415>
30. Lotfian S, Vikström T, Lennartsson A, Björkman B, Ahmed H, Samuelsson C (2019) Plastic-containing materials as alternative reductants for base metal production. *Can Metall Q* 58:164–176. <https://doi.org/10.1080/00084433.2018.1532951>
31. Isaksson J, Vikström T, Lennartsson A, Andersson A, Samuelsson C (2021) Settling of copper phases in lime modified iron silicate slag. *Metals* 11:1098. <https://doi.org/10.3390/met11071098>
32. Anton Paar GmbH F (2022). <https://www.anton-paar.com/corpen/products/details/furnace-rheometer-systems-frs-1600-and-frs-1800/>. Accessed 11 Mar 2022
33. Chen M, Raghunath S, Zhao B (2013) Viscosity of SiO₂-FeO-Al₂O₃ system in equilibrium with metallic Fe. *Metall Mater Trans B* 44:820–827. <https://doi.org/10.1007/s11663-013-9831-y>
34. Wang B, Yang H, Jin Z, Liu Z, Zou M (2022) Effect of Fe/SiO₂ ratio and Fe₂O₃ on the viscosity and slag structure of copper-smelting slags. *Metals* 12:24. <https://doi.org/10.3390/met12010024>
35. Jin Z, Wang B, Liu Z, Yang H, Zou M, Fu Y (2022) Effects of Fe/SiO₂ ratio and MgO content on the viscous behaviors of the SiO₂-FeO-MgO-12 Wt Pct Fe₂O₃-8 Wt Pct CaO-3 Wt Pct Al₂O₃ slag system. *Metall Mater Trans B* 53:902–915. <https://doi.org/10.1007/s11663-022-02432-6>
36. Lee Y, Dongjoon M, Jung S-M, Yi S (2004) Influence of basicity and FeO content on viscosity of blast furnace type slags containing FeO. *ISIJ Int* 44:1283–1290. <https://doi.org/10.2355/isijinternational.44.1283>
37. Lee S, Min DJ (2018) Viscous behavior of FeO-bearing slag melts considering structure of slag. *Steel Res Int* 89:1800055. <https://doi.org/10.1002/srin.201800055>
38. Deng L, Wang S, Zhang Z, Li Z, Jia R, Yun F, Li H, Ma Y, Wang W (2020) The viscosity and conductivity of the molten glass and crystallization behavior of the glass ceramics derived from stainless steel slag. *Mater Chem Phys* 251:123159. <https://doi.org/10.1016/j.matchemphys.2020.123159>
39. Ji F, Sichen D, Seetharaman S (1997) Experimental studies of the viscosities in the CaO-FeO-SiO₂ slags. *Metall Mater Trans B* 28:827–834. <https://doi.org/10.1007/s11663-997-0010-x>
40. Atkins P, De Paula J (2009) *Atkins physical chemistry*. Oxford University Press, Oxford
41. Urbain G, Bottinga Y, Richet P (1982) Viscosity of liquid silica, silicates and aluminosilicates. *Geochim Cosmochim Acta* 46:1061–1072. [https://doi.org/10.1016/0016-7037\(82\)90059-X](https://doi.org/10.1016/0016-7037(82)90059-X)
42. Roscoe R (1952) The viscosity of suspensions of rigid spheres. *Br J Appl Phys* 3:267. <https://doi.org/10.1088/0508-3443/3/8/306>
43. Manuel F-F, Pelaez-Ramirez H, López-Rodríguez J, Romero-Serrano A, Hernández-Ramírez A, Cruz-Ramírez A, Almaguer-Guzman I (2021) Effect of CaO/SiO₂ and Fe/SiO₂ ratios on the viscosity at 1300°C of partly crystallized silicate slags. *Glass Phys Chem* 47:75–82. <https://doi.org/10.1134/S1087659621020048>
44. Zhen YL, Zhang GH, Chou KC (2015) Viscosity of CaO-MgO-Al₂O₃-SiO₂-TiO₂ melts containing TiC particles. *Metall Mater Trans B* 46:155–161. <https://doi.org/10.1007/s11663-014-0169-x>
45. Bellemans I, Moelans N, Verbeken K (2015) Phase field modeling of the attachment of metallic droplets to solid particles in liquid slags: influence of interfacial energies and slag supersaturation. *Comput Mater Sci* 108:348–357. <https://doi.org/10.1016/j.commatsci.2015.03.019>
46. Bellemans I, Cnockaert V, De Wilde E, Moelans N, Verbeken K (2018) Metal droplet entrainment by solid particles in slags: an experimental approach. *J Sustain Metall* 4:15–32. <https://doi.org/10.1007/s40831-017-0145-1>
47. Bellemans I, De Wilde E, Blanpain B, Moelans N, Verbeken K (2017) Investigation of origin of attached Cu-Ag droplets to solid particles during high-temperature slag/copper/spinel interactions. *Metall Mater Trans B* 48:3058–3073. <https://doi.org/10.1007/s11663-017-1088-4>
48. Genevski K, Stefanova V (2008) Dispersed matte droplets in industrial slag melts from flash smelting furnace. *Can Metall Q* 47:51–58. <https://doi.org/10.1179/cm.2008.47.1.51>
49. Jalkanen H, Vehviläinen J, Poijärvi J (2003) Copper in solidified copper smelter slags. *Scand J Metall* 32:65–70. <https://doi.org/10.1034/j.1600-0692.2003.00536.x>
50. Coursol P, Valencia NC, Mackey P, Bell S, Davis B (2012) Minimization of copper losses in copper smelting slag during electric furnace treatment. *JOM* 64:1305–1313. <https://doi.org/10.1007/s11837-012-0454-6>

Publisher's Note Springer Nature remains neutral with regard to jurisdictional claims in published maps and institutional affiliations.

Authors and Affiliations

Jenny Isaksson¹  · Anton Andersson¹ · Tommy Vikström² · Andreas Lennartsson¹ · Caisa Samuelsson¹

✉ Jenny Isaksson
jenny.isaksson@ltu.se

¹ Division of Minerals and Metallurgical Engineering, Luleå University of Technology, 97 187 Luleå, Sweden

² Boliden Rönnskär, Skelleftehamn, 932 81 Skellefteå, Sweden